Tyrosine kinase epidermal cancer imaging: Mishani and Hagooly focus on strategies for molecular imaging and quantification of epidermal growth factor receptor–tyrosine kinase in cancer and outline the potential for these techniques in clinical practice. . . . . ***Page 1199***

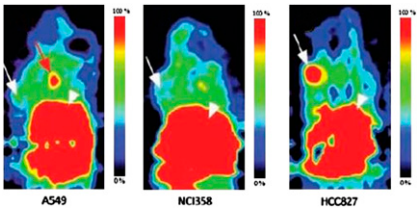

Significance of kinetic enhancement: Berridge provides perspective on the role of kinetic enhancement in radiopharmaceutical effectiveness and previews an article in this issue of *JNM* on the effect of radiopharmaceutical-to-serum protein binding on tracer kinetics. . . . ***Page 1203***

Preoperative PET in head and neck cancer: Rodrigues and colleagues compare optimized whole-body and dedicated high-resolution contrast-enhanced PET/CT protocols and contrast-enhanced CT in preoperative staging of primary squamous cell carcinoma of the head and neck. . . . . ***Page 1205***

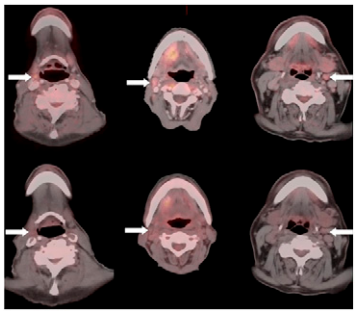

PET detection of bone metastases: Putzer and colleagues assess the comparative diagnostic values of CT imaging and somatostatin analog ^{68}Ga-DOTATOC PET in early detection of bone metastases from neuroendocrine tumors. . . . . ***Page 1214***

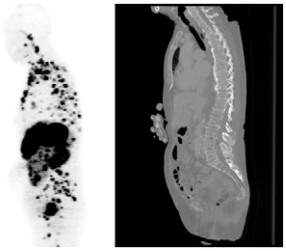

^{11}C-acetate uptake regulation in HCC: Yun and colleagues explore patterns of ^{11}C-acetate and ^{18}F-FDG uptake on PET/CT and expression of regulatory enzymes related to glycolysis and lipid synthesis in hepatocellular carcinoma. . . . ***Page 1222***

Receptor mapping with Hypotime: Møller and colleagues describe a method of calculation that uses ^{11}C-WAY washout rather than accumulation on PET to map serotonin $5HT_{1A}$ receptors in the human brain. . . . . ***Page 1229***

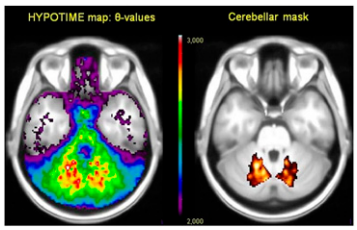

^{123}I-MIBG and ^{18}F-FDG in neuroblastoma: Sharp and colleagues assess differences in diagnostic utility of ^{123}I- MIBG scintigraphy and ^{18}F-FDG PET in patients with stages 1–4 neuroblastoma. . . . . ***Page 1237***

Parkin gene mutations and dopamine: Ribeiro and colleagues use ^{18}F-fluoro-L-DOPA, ^{11}C-PE2I, and ^{11}C-raclopride PET to characterize patterns of dopaminergic lesions and related clinical manifestations in young-onset Parkinson disease patients with and without mutations of the Parkin gene. . . . . ***Page 1244***

^{18}F-Flutemetamol PET: Nelissen and colleagues report on a phase 1 study of ^{18}F-flutemetamol, a thioflavin derivative of Pittsburgh compound B, including brain kinetic modeling, image acquisition optimization, and comparison of brain retention in Alzheimer disease patients and healthy controls. . . . . ***Page 1251***

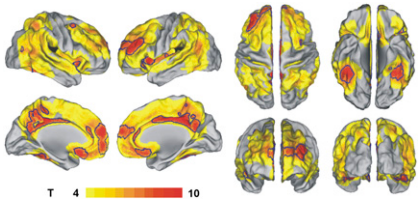

Altered serotonin transporters in AD: Ouchi and colleagues examine the relationship of clinical depression in early-to-moderate Alzheimer disease to changes in the brain serotoninergic system and glucose metabolism as assessed by ^{11}C-DASB and ^{18}F-FDG PET. . . . . ***Page 1260***

P-gp activity at the human BBB: Muzi and colleagues expand on previous studies designed to use ^{11}C-verapamil PET to image cyclosporine inhibition of multiple-drug resistance transporter P-glycoprotein activity at the blood–brain barrier in healthy humans. . . . . ***Page 1267***

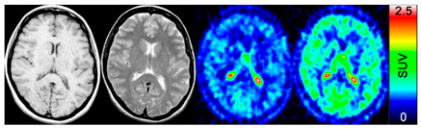

Novel translocator protein tracer: Endres and colleagues describe initial PET studies in humans with ^{11}C-DPA-713, a radioligand that binds to translocator proteins with high affinity, and discuss potential applications in assessment of neuroinflammation. . . . . ***Page 1276***

^{11}C-Methionine PET in MI: Morooka and colleagues examine whether ^{11}C-methionine localizes in areas of myocardial infarction after successful reperfusion and assess the

potential for PET imaging of the initial processes of remodeling. . . . . ***Page 1283***

Single-shot cardiorenal scintigraphy: Fommei and colleagues explore the hypothesis that a single combined cardiorenal ^{99m}Tc-tetrofosmin scintigraphy study can allow simultaneous investigation of cardiac and renal pathology in cardiovascular patients. . . . . ***Page 1288***

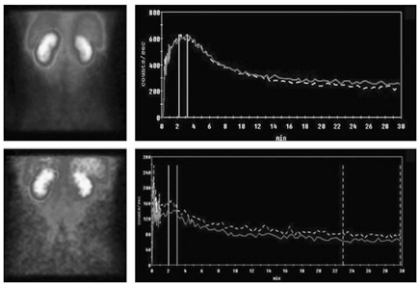

Predictive CAD testing: Shaw and Narula provide an educational overview of risk assessment, predictive accuracy, and economic outcomes for 3 commonly applied cardiac imaging procedures and highlight the potential added value of hybrid imaging. . . . . ***Page 1296***

Measuring spatial resolution in PET: Lodge and colleagues report on a quality assurance method for measuring spatial resolution in PET, designed to assist in standardization of data collection for enhanced comparison of results, particularly those from multicenter trials. . . . ***Page 1307***

TOF PET tumor detectability: Kadrmas and colleagues evaluate the effect of time-of-flight technology on observer performance in detecting and localizing focal warm lesions in noisy PET images acquired in an anthropomorphic phantom. . . . . ***Page 1315***

Kinetic model for CSF RIT delivery: Lv and colleagues describe a pharmacokinetic model to evaluate the role of kinetic and transport parameters of radioimmunotherapy designed to treat leptomeningeal metastases using antibodies administered directly into the cerebrospinal fluid. . . . . ***Page 1324***

MDR1 influences ^{64}Cu-ATSM retention: Liu and colleagues investigate the role of multidrug resistance type 1 protein expression in accumulation and retention of two ^{64}C-labeled tracers and discuss the implications for imaging of tumor hypoxia. . . . . ***Page 1332***

SPECT/CT and *HER2* expression: McLarty and colleagues describe animal studies on ^{111}In-DTPA-pertuzumab SPECT detection of early molecular response to trastuzumab as indicated by *HER2* downregulation and of tumor response with decreased numbers of *HER2*-positive viable tumor cells. . . . . ***Page 1340***

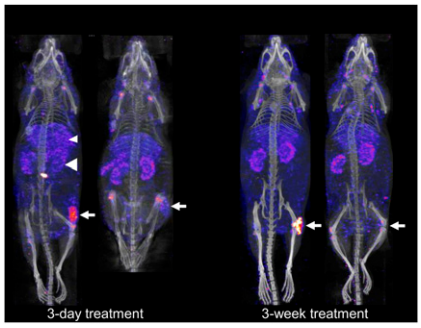

Central nAChR tracer: Valette and colleagues report on in vitro characterization and in vivo primate studies of a novel radioligand for PET imaging of central nicotinic acetylcholine receptors. . . . . ***Page 1349***

Quantitative imaging of angiogenesis: Dobrucki and colleagues report on validation studies of a semiautomated approach for serial quantitative evaluation of peripheral angiogenesis with micro-SPECT/CT. . . . . ***Page 1356***

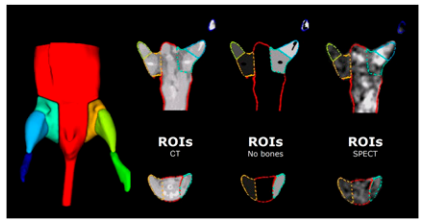

K-Ras and uptake in thyroid cancer: Prante and colleagues explore molecular mechanisms behind increases in ^{18}F-FDG uptake on PET imaging in dedifferentiated thyroid cancer, with findings that point to oncogene activation of intracellular signal transduction cascades. . . . . ***Page 1364***

Apoptosis in right ventricular disease: Campian and colleagues study the role of apoptosis in this setting by monitoring disease progression and treatment response with ^{99m}Tc-annexin-V scintigraphy in rats. . . . . ***Page 1371***

Serum protein binding of ^{123}I-IMP: Kuga and colleagues investigate whether amino acid infusion can improve cerebral accumulation of this SPECT tracer by competitive displacement of serum protein binding. . . . . ***Page 1378***

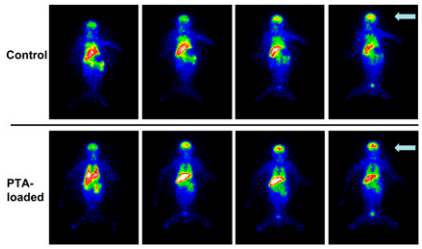

ON THE COVER

Time-of-flight PET significantly improves observer performance in detecting focal lesions on a noisy background, as illustrated by this ^{18}F-FDG PET/CT scan of a patient with esophageal cancer and a body mass index of 27. The reconstructions that include time-of-flight information show improved uniformity in the liver and mediastinal region and better delineate the bone marrow in the ribs and spine.

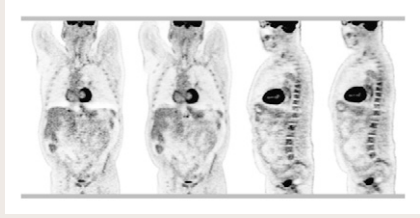

See page 1322.